Letter

Tunable Multimode Lasing in a Fiber Ring

Eyal Buks*

Andrew and Erna Viterbi Department of Electrical Engineering, Technion, Haifa 32000, Israel

(Received 11 January 2023; revised 18 January 2023; accepted 14 April 2023; published 8 May 2023)

We experimentally study a fiber loop laser with an integrated erbium-doped fiber (EDF). The output optical spectrum is measured as a function of the EDF temperature. We find that below a critical temperature of about 10 K the measured optical spectrum exhibits a sequence of narrow and unequally spaced peaks. Externally injected light and filtering are employed for tuning the peaks' wavelengths. Operation of the device as an optical memory having a storage time of about 20 ms is demonstrated. The multimode lasing tunability can be exploited for novel applications in the fields of sensing, communication, and quantum data storage.

DOI: 10.1103/PhysRevApplied.19.L051001

Introduction.—Erbium-doped fibers (EDFs) are widely employed in a variety of applications. Key properties of EDFs can be controlled by varying the temperature [1–3]. Multimode lasing has a variety of applications in the fields of sensing, spectroscopy, signal processing, and communication [4]. Multimode lasing in the telecom band has been demonstrated by integrating an EDF cooled by liquid nitrogen into a fiber ring laser [5–7]. It has been recently proposed that EDFs operating at low temperatures can be used for storing quantum information [8–13]. Population storage times exceeding 10 s [14], and electronic spin lifetimes exceeding one hour [15], have been demonstrated using persistent spectral hole burning.

In this work we study a fiber loop laser with an integrated EDF [16,17]. We measure the emitted optical spectrum as a function of the EDF temperature [18,19]. Below a critical temperature of about 10 K the measured optical spectrum exhibits an unequally spaced optical comb (USOC) made of a sequence of narrow peaks. The observed USOC and multimode lasing are attributed to intermode coupling [20,21]. We find that the wavelengths at which the multimode lasing occurs can be controlled by light that is externally injected into the fiber loop. The possibility of using the device under study as an optical memory is explored, and a storage time of about 20 ms is demonstrated. The USOC controllability, together with its high stability, can be exploited for facilitating novel applications in the fields of sensing, communication, and quantum data storage.

Experimental Setup.—The experimental setup is schematically depicted in Fig. 1(a). An EDF having length of 20 m, absorption of 30 dB m^{-1} at 1530 nm, and mode field diameter of 6.5 μm at 1550 nm is cooled down using a cryogen-free cryostat. The EDF is thermally coupled to a calibrated silicon diode serving as a thermometer, and it is pumped using a 980-nm laser diode (LD) biased with current denoted by I_D. The cold EDF is integrated with a room-temperature fiber loop using a wavelength-division multiplexing (WDM) device. Two isolators [labeled by arrows in the sketch shown in Fig. 1(a)] and a 10:90 output coupler (OC) are integrated in the fiber loop. The loop frequency f_L (inverse loop period time), which is measured using a radio frequency spectrum analyzer and a photodetector, is given by $f_L = c/(n_F l_L) = 4.963$ MHz, where c is the speed of light in vacuum, $n_F = 1.45$ is the fiber refractive index, and $l_L = 41.7$ m is the fiber loop total length. An optical spectrum analyzer (OSA) is connected to the 10:90 OC.

USOC.—Near a wavelength of 1540 nm and below a critical temperature of about 10 K the measured optical spectrum exhibits narrow peaks at a sequence of wavelengths denoted by $\{\lambda_n\}$, where $n = 0, 1, 2, \ldots$ [see Fig. 1(b)]. For the data presented in Fig. 1, $\lambda_0 = 1540.629$ nm and $\lambda_1 - \lambda_0 = 0.1661$ nm. The frequency f_n associated with wavelength λ_n is given by $f_n = c/\lambda_n$. The intensity of the USOC peak occurring at wavelength λ_n is denoted by I_n.

The normalized frequency sequence $i_n \equiv (f_0 - f_n)/f_L$ and the normalized intensity sequence $s_n \equiv I_n/I_1$ are well described by the following empirical laws:

$$i_n = \nu \log p_n, \tag{1}$$

$$s_n = \frac{\lambda_{n+1} - \lambda_n}{\lambda_1 - \lambda_0}, \tag{2}$$

*eyal@ee.technion.ac.il

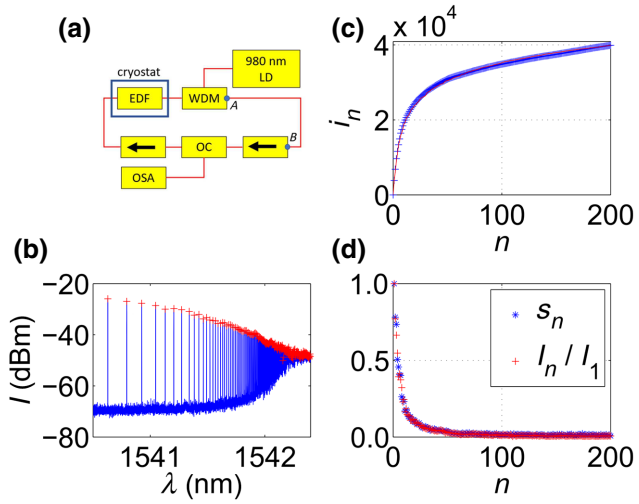

FIG. 1. USOC. (a) The experimental setup. (b) The measured optical spectrum with diode current $I_D = 120$ mA. (c) Comparison between the measured normalized frequencies $i_n = (f_0 - f_n)/f_L$ and the calculated values of $\nu \log p_n$ [see Eq. (1)]. The dimensionless prefactor ν is found by fitting to be given by $\nu = 5610$. (d) Comparison between the normalized intensities I_n/I_1 and the normalized wavelength gaps $(\lambda_{n+1} - \lambda_n) / (\lambda_1 - \lambda_0)$ [see Eq. (2)].

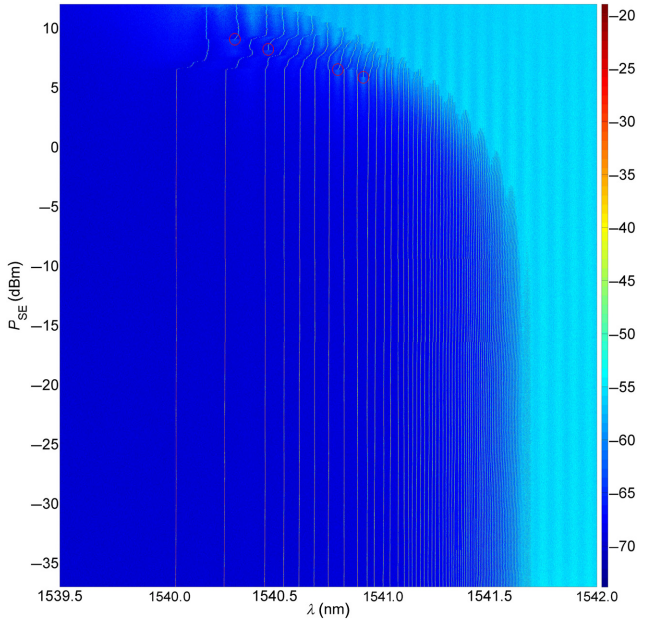

FIG. 2. Gain saturation. Optical spectrum (in dBm) as a function of the SE optical power P_{SE} feeding the 1:99 OC. The temperature is $T = 2.9$ K and diode current is $I_D = 100$ mA.

where ν is a positive constant and p_n is the nth prime number. The comparison between the measured values of $i_n = (f_0 - f_n)/f_L$ and the calculated values of $\nu \log p_n$ [see Eq. (1)] yields a good agreement [see Fig. 1(c)]. The level of agreement is quantified by the parameter $\varepsilon = n_m^{-1} \sum_{n=1}^{n_m} \left| (i_n - \nu \log p_n)/i_{n_m} \right|$, where n_m is the number of peaks that can be reliably resolved. For the data shown in Fig. 1, $n_m = 200$ and $\varepsilon = 0.0043$. The comparison between I_n/I_1 and $(\lambda_{n+1} - \lambda_n) / (\lambda_1 - \lambda_0)$ [see Eq. (2)] is shown in Fig. 1(d). The underlying mechanism responsible for USOC formation remains mainly unknown. The connection between the normalized frequency sequence $i_n = (f_0 - f_n)/f_L$ and the sequence of prime numbers [see Eq. (1)] is discussed in Ref. [21].

Gain saturation.—The fiber loop gain can be characterized by injecting input light having a continuous spectrum. Injection measurements (shown in Figs. 2, 3, and 4) are performed by integrating a 1:99 OC into the loop between the points labeled as "A" and "B" in Fig. 1(a). For the measurements presented in Fig. 2, the 1:99 OC is employed to inject into the loop spontaneous emission (SE) light from an external pumped EDF. The optical power of the externally injected SE light is controlled by a tunable attenuator. The plot shown in Fig. 2 exhibits the spectrum measured by the OSA as a function of the SE optical power P_{SE} feeding the 1:99 OC.

Consider two neighboring USOC peaks at wavelengths λ_n and λ_{n+1}, where n is a non-negative integer. As can be seen from Fig. 2, the loop gain g_L in the region $[\lambda_n, \lambda_{n+1}]$ is approximately a symmetric function around the midpoint $\lambda_{a,n} = (\lambda_n + \lambda_{n+1})/2$, at which g_L peaks. The loop gain g_{L} vanishes at the end points λ_n and λ_{n+1}.

When the SE input optical power P_{SE} is sufficiently high, new USOC peaks at the midpoint wavelengths $\lambda_{a,n}$ are created (see the regions highlighted by the overlaid red circles in Fig. 2). This behavior is attributed to the fact that the wavelengths λ_n and λ_{n+1}, together with the midpoint wavelength $\lambda_{a,n}$, nearly satisfy the mixing condition $f_n + f_{n+1} = 2f_{a,n}$, where $f_{a,n} = c/\lambda_{a,n}$ (recall that $|\lambda_{n+1} - \lambda_n| \ll \lambda_n$). Note that the USOC created with relatively intense SE injection (see Fig. 2) is significantly distorted, and it cannot be well described by the empirical laws (1) and (2).

Laser Injection.—The plot shown in Fig. 3 demonstrates external tuning of an USOC peak. For the measurements presented in Fig. 3, the 1:99 OC is fed with a narrow-band external laser having a tunable wavelength λ_L. The experimental protocol has three steps. In the first one the external laser having wavelength λ_L is turned on, then in the second step the diode current is turned on, and in the last step the external laser is turned off. After each step the optical spectrum is measured. The measured spectra after the first, second, and third steps are shown in the plots in Fig. 3 labeled by the numbers 1, 2, and 3, respectively.

In some cases, the spectrum that is measured after the third step, i.e., after turning off the external laser, contains a peak at the injected external laser wavelength λ_L. This is demonstrated by plots in Figs. 3(b) and 3(c). We find that this persistent effect occurs only when λ_L is tuned inside the USOC region of about 1540–1542.5 nm [compare with

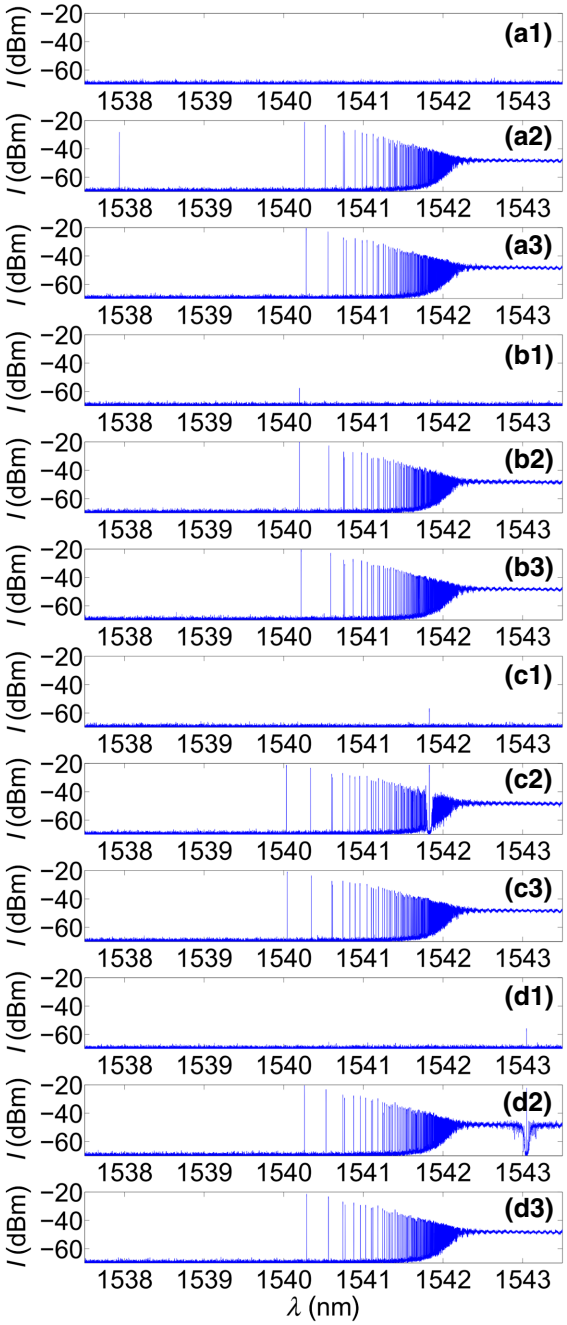

FIG. 3. Laser injection. The measured optical spectrum after the first (1), second (2), and third (3) step. The monochromatic injected light of the external laser has wavelength λ_L of (a) $\lambda_L =$ 1537.917 nm, (b) $\lambda_L = 1540.162$ nm, (c) $\lambda_L = 1541.784$ nm, and (d) $\lambda_L = 1543.000$ nm. The temperature is $T = 3.0$ K, diode current is $I_D = 200$ mA, and tunable laser power is 0.1 mW.

the plots in Figs. 3(a) and 3(d), for which the persistent effect does not occur].

Moving a single peak.—Each USOC peak wavelength λ_n can be individually tuned using external laser injection. The tuning method is demonstrated for the second ($n = 1$)

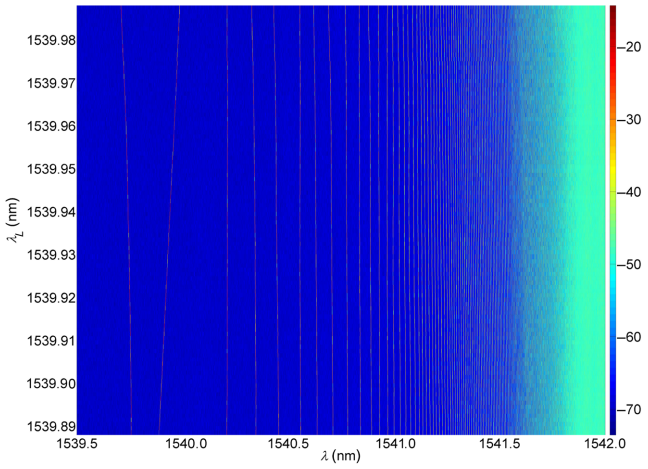

FIG. 4. Peak moving. The tunable laser wavelength λ_L is varied from 1539.988 to 1539.888 nm in steps of 1 pm. During the time when the wavelength λ_L is modified, the external laser optical power is turned off (using an external attenuator). The measured optical spectrum is shown in dBm as a function of λ_L. The temperature is $T = 2.9$ K, diode current is $I_D = 200$ mA, and tunable laser power is 0.39 mW.

USOC peak in Fig. 4. Peak moving is achieved by first tuning the external laser wavelength λ_L to match the USOC peak wavelength to be moved λ_n, and then by gradually tuning λ_L to a target value denoted by $\lambda_{n,T}$. After reaching the target value, the external laser is switched off. For the example shown in Fig. 4, all peaks with $n > 1$ are unaffected by the moving process applied to the $n = 1$ peak.

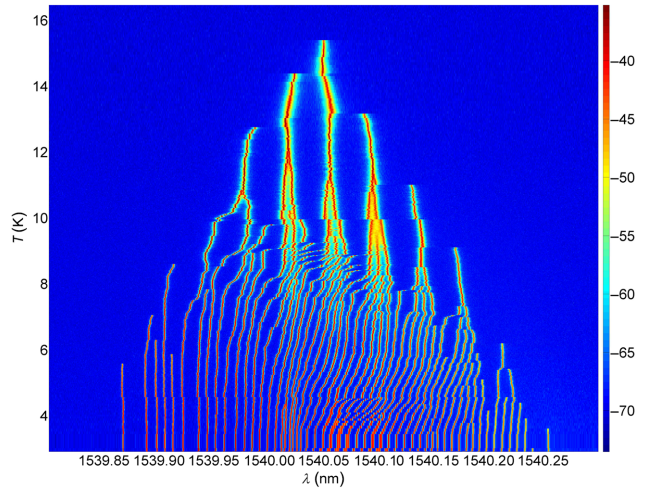

FIG. 5. Optical filter. A tunable filter is integrated into the fiber loop. The plot displays the optical spectrum (in dBm) as a function of temperature T. The optical filter central wavelength λ_F is tuned to the value $\lambda_F = 1540$ nm and the diode current is set to $I_D = 100$ mA.

The moving of the USOC nth peak is possible when the external laser power P_L exceeds a threshold value denoted by P_n. By carefully tuning P_L (to be sufficiently close to P_n), the tuning process of the nth peak wavelength from the initial value λ_n to the target value $\lambda_{n,T}$ can be performed without affecting the wavelengths $\lambda_{n'}$ of all other USOC peaks having $n' \neq n$.

Optical filter.—The band inside which USOC occurs can be controlled using an optical filter. For the measurement shown in Fig. 5, a Fabry-Perot filter having full width at half maximum of 1.2 nm is integrated into the loop between the points "A" and "B" [see the sketch in Fig. 1(a)]. The plot shown in Fig. 5, which exhibits the temperature dependence of the created USOC, demonstrates a transition from low-temperature multimode lasing to higher-temperature single-mode lasing. Note that the same above-discussed tuning methods (see Figs. 3 and 4) can be successfully implemented to manipulate the peaks of the filtered USOC shown in Fig. 5.

Memory.—The USOC wavelength sequence $\{\lambda_n\}$ is highly stable. Over time periods exceeding 20 h, changes in the sequence $\{\lambda_n\}$ are too small to be reliably resolved by our OSA, provided that the 980-nm LD bias current I_D is kept constant. However, the sequence $\{\lambda_n\}$ is significantly modified each time I_D is switched off, and then switched on again, provided that the off time τ_{off} is sufficiently long. On the other hand, we find that the sequence $\{\lambda_n\}$ remains unchanged when τ_{off} is sufficiently short.

Amplitude modulation applied to the LD bias current I_D is employed to determine the USOC memory time, which is denoted by τ_M. This is done by measuring the sequence $\{\lambda_n\}$ before and after a switching-off pulse having time duration τ_{off} is applied to I_D. We find that when $\tau_{\text{off}} \ll \tau_M$, the sequence $\{\lambda_n\}$ is unaffected by the off pulse, where $\tau_M \simeq 20$ ms. On the other hand, $\{\lambda_n\}$ is significantly modified for $\tau_{\text{off}} \gg \tau_M$. In the region where $\tau_{\text{off}} \simeq 20$ ms, we find that most of the wavelengths in the sequence $\{\lambda_n\}$ remain unchanged, except for the first and/or the second ones (having the shortest wavelengths). This behavior is demonstrated by the plots shown in Fig. 6, for which the off time is $\tau_{\text{off}} = 22$ ms. For this case, the off pulse shifts the first wavelength λ_0 by -65 pm, and all other peaks are nearly unaffected. Note that the memory time τ_M is expected to strongly depend on the temperature [8–15].

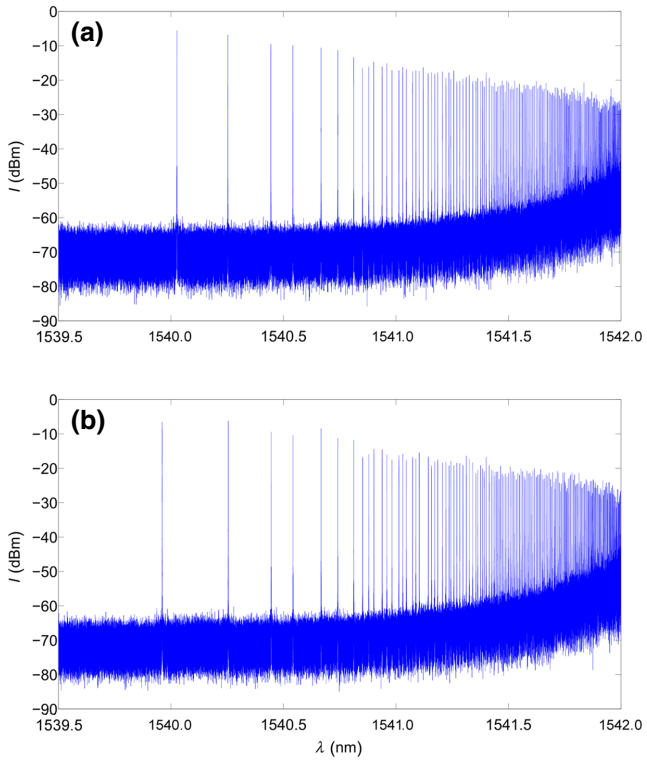

FIG. 6. USOC memory. Optical spectrum before (a) and after (b) an off pulse having time duration of $\tau_{\text{off}} = 22$ ms. In our experimental setup, the LD bias current I_D can be fully modulated with frequency of up to about 150 kHz. Diode current (before and after the off pulse) is $I_D = 150$ mA and temperature is $T = 3.5$ K.

Summary.—Further study is needed to reveal the underlying mechanism responsible for the USOC formation. Our measurements demonstrate several methods that allow tuning of the wavelengths at which multimode lasing occurs. Future study will focus on systematically characterizing spectral hole burning [22] in the system under study, in order to explore its performance for quantum memory applications.

Acknowledgments.—We thank Tian Zhong for useful discussions. This work is supported by the Israeli Science Foundation.

[1] Andrey Kobyakov, Michael Sauer, and Dipak Chowdhury, Stimulated Brillouin scattering in optical fibers, Adv. Opt. Photonics **2**, 1 (2010).

[2] Julien Le Gouët, Jérémy Oudin, Philippe Perrault, Alaeddine Abbes, Alice Odier, and Alizée Dubois, On the effect of low temperatures on the maximum output power of a coherent erbium-doped fiber amplifier, J. Lightwave Technol. **37**, 3611 (2019).

[3] Luc Thevenaz, Alexandre Fellay, Massimo Facchini, Walter Scandale, Marc Nikles, and Philippe A Robert, in *Smart Structures and Materials 2002: Smart Sensor Technology and Measurement Systems*. (International Society for Optics and Photonics, 2002), vol. 4694, p. 22.

[4] Hermann Haken, *Laser Light Dynamics* (North-Holland Amsterdam, 1985), Vol. 1.

[5] S. Yamashita and K. Hotate, Multiwavelength erbium-doped fibre laser using intracavity etalon and cooled by liquid nitrogen, Electron. Lett. **32**, 1298 (1996).

[6] Haochong Liu, Wei He, Yantao Liu, Yunhui Dong, and Lianqing Zhu, Erbium-doped fiber laser based on

femtosecond laser inscribed FBG through fiber coating for strain sensing in liquid nitrogen environment, Opt. Fiber Technol. **72**, 102988 (2022).

[7] J. Lopez, H. Kerbertt, M. Plata, E. Hernandez, and S. Stepanov, Two-wave mixing in erbium-doped-fibers with spectral-hole burning at 77 K, J. Opt. **22**, 085401 (2020).

[8] Erhan Saglamyurek, Jeongwan Jin, Varun B. Verma, Matthew D. Shaw, Francesco Marsili, Sae Woo Nam, Daniel Oblak, and Wolfgang Tittel, Quantum storage of entangled telecom-wavelength photons in an erbium-doped optical fibre, Nat. Photonics **9**, 83 (2015).

[9] Matthias U. Staudt, Sara R. Hastings-Simon, Mikael Afzelius, Didier Jaccard, Wolfgang Tittel, and Nicolas Gisin, Investigations of optical coherence properties in an erbium-doped silicate fiber for quantum state storage, Opt. Commun. **266**, 720 (2006).

[10] Shi-Hai Wei, Bo Jing, Xue-Ying Zhang, Jin-Yu Liao, Hao Li, Li-Xing You, Zhen Wang, You Wang, Guang-Wei Deng, and Hai-Zhi Song *et al.*, Storage of 1650 modes of single photons at telecom wavelength, arXiv:2209.00802 (2022).

[11] Antonio Ortu, Jelena V. Rakonjac, Adrian Holzäpfel, Alessandro Seri, Samuele Grandi, Margherita Mazzera, Hugues de Riedmatten, and Mikael Afzelius, Multimode capacity of atomic-frequency comb quantum memories, Quantum Sci. Technol. **7**, 035024 (2022).

[12] Duan-Cheng Liu, Pei-Yun Li, Tian-Xiang Zhu, Liang Zheng, Jian-Yin Huang, Zong-Quan Zhou, Chuan-Feng Li, and Guang-Can Guo, On-demand storage of photonic qubits at telecom wavelengths, arXiv:2201.03692 (2022).

[13] Lucile Veissier, Mohsen Falamarzi, Thomas Lutz, Erhan Saglamyurek, Charles W. Thiel, Rufus L. Cone, and Wolfgang Tittel, Optical decoherence and spectral diffusion in an erbium-doped silica glass fiber featuring long-lived spin sublevels, Phys. Rev. B **94**, 195138 (2016).

[14] Erhan Saglamyurek, Thomas Lutz, Lucile Veissier, Morgan P. Hedges, Charles W. Thiel, Rufus L. Cone, and Wolfgang Tittel, Efficient and long-lived Zeeman-sublevel atomic population storage in an erbium-doped glass fiber, Phys. Rev. B **92**, 241111 (2015).

[15] Sara Shafiei, Erhan Saglamyurek, and Daniel Oblak, in *Quantum Information and Measurement*. (Optical Society of America, 2021), p. F2A–4.

[16] Andris Antuzevics, Epr characterization of erbium in glasses and glass ceramics, Low Temp. Phys. **46**, 1149 (2020).

[17] Hermann Haken, *Laser Light Dynamics* (North-Holland Amsterdam, 1985), Vol. 2.

[18] Marine Aubry, Luciano Mescia, Adriana Morana, Thierry Robin, Arnaud Laurent, Julien Mekki, Emmanuel Marin, Youcef Ouerdane, Sylvain Girard, and Aziz Boukenter, Temperature influence on the radiation responses of erbium-doped fiber amplifiers, Phys. Status Solidi (A) **218**, 2100002 (2021).

[19] João Paulo Lebarck Pizzaia, Rodolpho Ladislau Silva, Arnaldo Gomes Leal-Junior, and Carlos Eduardo Schmidt Castellani, Temperature sensor based on an erbium-doped fiber Sagnac interferometer, Appl. Opt. **61**, 2352 (2022).

[20] Jerome Moloney and Alan Newell, *Nonlinear Optics* (CRC Press, 2018).

[21] Eyal Buks, Low temperature spectrum of a fiber loop laser, Phys. Lett. A **458**, 128591 (2023).

[22] Inga L. Rittner and Peter M. Krummrich, in *Photonic Networks; 22th ITG Symposium* (VDE, 2021), p. 1.